Available online at www.sciencedirect.com
ScienceDirect
Journal of Sound and Vibration 297 (2006) 1025–1047
JOURNAL OF SOUND AND VIBRATION
www.elsevier.com/locate/jsvi

Acoustical wave propagator technique for time-domain reflection and transmission of flexural wave packets in one-dimensional stepped beams ☆

S.Z. Peng[a,*], J. Pan[b]

[a]*Department of Mechanical Engineering, The Hong Kong Polytechnic University, Hung Hom, Kowloon, Hong Kong, Hong Kong*
[b]*Centre for Acoustics, Dynamics and Vibration, School of Mechanical Engineering, The University of Western Australia, 35 Stirling HWY, Crawley, WA 6009, Australia*

Received 26 July 2005; received in revised form 24 March 2006; accepted 8 May 2006
Available online 27 June 2006

Abstract

This paper applies the acoustical wave propagator technique to wave packet propagation in a one-dimensional stepped beam. The time-domain analytical solutions of this structure subjected to an initial-value problem with the specific Gaussian waveform were derived and compared with the predicted results obtained by the acoustical wave propagator technique. It is shown that this technique is efficient and accurate in predicting wave propagation in one-dimensional structure with thickness discontinuity. The effects of near-field waves on reflection and transmission coefficients, and transmission efficiencies are also studied in detail. Furthermore, an experiment was carried out to investigate the reflection and transmission of flexural waves in a stepped beam structure.

1. Introduction

Beams and struts are important structural elements and form the basis of many engineering frameworks commonly found in shipbuilding, nuclear and aerospace industries. Wave propagation and reflection of elastic waves in beams at discontinuities have recently received significant attention. Sato [1] studied free vibration of beams with abrupt changes of cross-section. Afterwards, Doyle and his colleagues [2–3] used the exact (frequency-dependent) dynamic stiffness matrix to investigate wave propagation in structures in conjunction with the spectral analytical method. Lee [4–6] introduced the spectral transfer matrix method to investigate vibration analysis of one-dimensional structures. Recently, Wang and Rose [7] presented an analytical approach using higher-order plate theories to determine wave reflections and transmissions in beams containing inhomogeneity. However, in many structures with discontinuities, exact analytical solutions of time-domain wave motion are not available. It is therefore necessary to develop an effective and accurate numerical method.

☆Part of the paper has been presented at the 18th International Congress on Acoustics, April 4–9, Kyoto, Japan, 2004.
*Corresponding author. Tel.: +852 2766 6664; fax: +852 2365 4703.
E-mail addresses: mmszpeng@polyu.edu.hk (S.Z. Peng), pan@mech.uwa.edu.au (J. Pan).

0022-460X/$ - see front matter © 2006 Elsevier Ltd. All rights reserved.
doi:10.1016/j.jsv.2006.05.005

Most recently, Peng and Pan [8–12] applied the acoustical wave propagator (AWP) technique developed by Pan and Wang [13] to study the time-domain wave propagation and dynamic stress concentration in two-dimensional plate structures. Their work showed that the AWP technique combining the Chebyshev polynomial expansions with fast Fourier transformation is highly accurate and computationally efficient. The main motivation of this paper focuses on applying the AWP technique to flexural wave motion in one-dimensional beam structures, and extending this technique to study reflection and transmission coefficients and energy flow in a beam with a sharp change of section. In addition, the effects of the near-field waves on the predicted results together with the thickness ratio of the beams on reflection and transmission in the vicinity of the discontinuity boundary of the beam are studied in detail. Furthermore, the exact analytical solutions of this structure impacted by an initial Gaussian wave packet are derived to compare with the predicted results from the AWP technique. Finally, an experiment concerning the reflection and transmission of flexural wave in a stepped beam structure with a finite beam and semi-infinite beam is presented and compared with predictions based on the AWP technique.

2. Theory of the acoustical wave propagator technique in one-dimensional structures

2.1. Derivatives of the acoustical wave propagator $e^{-(t-t_0)\hat{\mathbf{H}}}$

Consider a long thin beam with different cross-sections undergoing transverse motion as illustrated in Fig. 1. This stepped beam structure is regarded as a common component of many practical engineering structures due to a number of attractive features, such as material saving, weight reduction, stiffness enhancing, designated strengthening, etc. Three assumptions are made in this paper: the width of the beam is much less than its length; Poisson's effect can be neglected; and the plane cross-sections initially perpendicular to the axis of the beam remain plane and perpendicular to the neutral axis during bending.

According to the relationship between the bending moment and curvature, we have

$$\frac{\partial M}{\partial t} = -EI\frac{\partial^2 V}{\partial x^2}, \tag{1}$$

where

$$E = E(x) = \begin{cases} E_1 \\ E_2 \end{cases}$$

E_1 and E_2 represent the Young's moduli of sub-beams 1 and 2, respectively; and

$$I = I(x) = \begin{cases} I_1 \\ I_2 \end{cases}$$

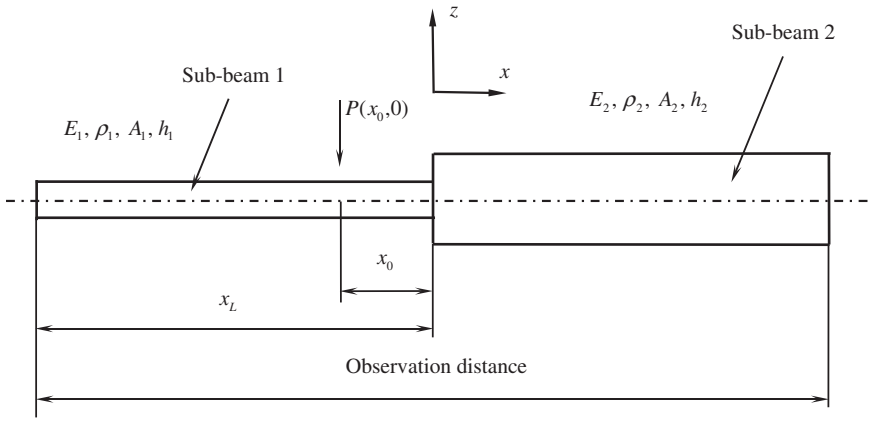

Fig. 1. Schematic of a stepped beam structure.

I_1 and I_2 represent the cross-sectional area moments of inertia of sub-beams 1 and 2, respectively; $V(x,t) = \partial W/\partial t$ is the velocity of the beam along the z-direction; and $W(x, t)$ is the displacement of the beam in the z-direction.

The governing equation for the motion of the structure is given by

$$\rho A \frac{\partial^2 W}{\partial t^2} = \frac{\partial^2 M}{\partial x^2} + P(x_0, t), \tag{2}$$

where

$$\rho = \rho(x) = \begin{cases} \rho_1 \\ \rho_2 \end{cases}$$

ρ_1 and ρ_2 represent the densities of sub-beams 1 and 2, respectively; and

$$A = A(x) = \begin{cases} A_1 \\ A_2 \end{cases}$$

A_1 and A_2 represent the cross-sectional areas of sub-beams 1 and 2, respectively; and $P(x_0, t)$ is a distributed force. In this paper, only the time-dependent response to initial conditions is discussed. In this case, $P(x_0, t) = 0$.

Thus, the derivative of the shear force Q with respect to time can be calculated by

$$\frac{\partial Q}{\partial t} = -EI \frac{\partial^3 V}{\partial x^3}.$$

The system state equation can be described by the following form:

$$\frac{\partial}{\partial t}\Phi(x, t) = -\hat{\mathbf{H}}\Phi(x, t), \tag{3}$$

where $\Phi(x, t)$ is a state vector representing the velocity $V(x, t)$ and bending moment $M(x, t)$, defined as

$$\Phi(x, t) = [\, V \quad M \,]^{\mathrm{T}} \tag{4}$$

and $\hat{\mathbf{H}}$ is the system operator defined as

$$\hat{\mathbf{H}} = \begin{bmatrix} 0 & -\frac{1}{\rho A}\frac{\partial^2}{\partial x^2} \\ EI\frac{\partial^2}{\partial x^2} & 0 \end{bmatrix}. \tag{5}$$

Eq. (3) can be rewritten by integrating with respect to time

$$\Phi(x, t) = \mathrm{e}^{-(t-t_0)\hat{\mathbf{H}}}\Phi(x, t_0), \tag{6}$$

where $\mathrm{e}^{-(t-t_0)\hat{\mathbf{H}}}$ is named as the AWP and $\Phi(x, t_0)$ denotes the initial state vector.

Through the operation of the AWP $\mathrm{e}^{-(t-t_0)\hat{\mathbf{H}}}$ acting upon the initial state vector, we can obtain the state vector $\Phi(x, t)$ of the acoustical waves at any time t and any position x. In Eq. (5), the material properties E, ρ, A and h are functions of position. It is those position-dependent system parameters, which give rise to the effect of boundaries at the coupling interface of the component beams.

2.2. *Implementation of the acoustical wave propagator* $\mathrm{e}^{-(t-t_0)\hat{\mathbf{H}}}$

The crucial step in numerical implementation is the development of an efficient algorithm for performing the operation of the AWP. The Chebyshev polynomial expansion (CPE) scheme has the significant advantage that it allows the use of a very long time step. In addition, this scheme has an exponential convergent rate. More detailed accounts can be found in the Refs. [8,9]. Real Chebyshev polynomials defined in the ranges of $[-1,1]$ are used in the expansion of the AWP. To ensure the convergence of the Chebyshev expansion, the

system operation $\hat{\mathbf{H}}$ needs to be normalized by $\hat{\mathbf{H}}' = \hat{\mathbf{H}}/\lambda_{\max}$, where $\lambda_{\max}$ represents the maximum eigenvalue of the system operator $\hat{\mathbf{H}}$.

Using Chebyshev polynomials of the first kind, Eq. (6) can be further rewritten as

$$\Phi(x,t) = \left[I_0(R)I + 2I_1(R)\hat{\mathbf{H}}' + 2\sum_{n=2}^{\infty} I_n(R)T_n(\hat{\mathbf{H}}') \right] \Phi(x,t_0), \tag{7}$$

where $R = \lambda_{\max}(t-t_0)$; and $I_n(R)$ is the nth-order modified Bessel function of the first kind. The Chebyshev polynomials $T_n\left(\hat{\mathbf{H}}'\right)$ can be obtained by the recursive formula

$$T_{n+1}\left(\hat{\mathbf{H}}'\right) = 2\hat{\mathbf{H}}' T_n\left(\hat{\mathbf{H}}'\right) - T_{n-1}\left(\hat{\mathbf{H}}'\right), \quad \text{where } n \geqslant 2. \tag{8}$$

In this paper, the following Fourier transformation and its inverse transformation are used to calculate the spatial derivatives of function $\Phi(x,t)$:

$$\frac{\partial^2}{\partial x^2}\Phi(x,t) = F^{-1}\left\{(\mathrm{i}k_x)^2 F[\Phi(x,t)]\right\}, \tag{9}$$

where $\mathrm{i} = \sqrt{-1}$; $F^{-1}\{\}$ and $F[\ ]$ represent the inverse Fourier transformation and Fourier transformation, respectively; and k_x is the bending wavenumber along the x-direction. It is noting that Eq. (9) is only given for the flexural wave components. For near-field wave components, the only difference is reflected by the minus sign "−", as given by

$$\frac{\partial^2}{\partial x^2}\Phi(x,t) = F^{-1}\left\{(k_x)^2 F[\Phi(x,t)]\right\}.$$

The error analysis of the Fourier transformation method for the spatial derivatives has been given in Ref. [13] to compare with other numerical schemes.

If the spatial sampling interval Δx is chosen to represent the highest frequency component of interest in the medium, then the bending wave velocity c_B can be calculated by $c_B = \omega/k_x = \{1.8c_L hf\}^{1/2}$, where c_L and f represent the longitudinal wave velocity and frequency, respectively; and

$$h = h(x) = \begin{cases} h_1 \\ h_2 \end{cases}$$

h_1 and h_2 represent the thickness of sub-beams 1 and 2, respectively. In addition, the normalization factor R can be calculated by

$$R = \lambda_{\max}(t-t_0) = \sqrt{\frac{EI}{\rho A}}\left(\frac{\pi}{\Delta x}\right)^2 (t-t_0). \tag{10}$$

2.3. Reflection and transmission coefficients and exact analytical solutions of a stepped beam structure

The prediction accuracy of the Chebyshev–Fourier Scheme developed in the previous section can be assessed by the exact analytical solutions. The flexural waves in beams have two fundamentally different modal solutions, which consist of both propagating and evanescent terms. It is useful to analyse the transmission and reflection of wave packets at a step discontinuity in both cross-sectional area and material properties, as illustrated in Fig. 2. The elementary differential equation of motion for bending waves can be represented by

$$\begin{aligned} E_1 I_1 \frac{\partial^4 W_1}{\partial x^4} - \rho_1 A_1 \frac{\partial^2 W_1}{\partial t^2} = 0, \quad x \leqslant 0, \\ E_2 I_2 \frac{\partial^4 W_2}{\partial x^4} - \rho_2 A_2 \frac{\partial^2 W_2}{\partial t^2} = 0, \quad x \geqslant 0, \end{aligned} \tag{11}$$

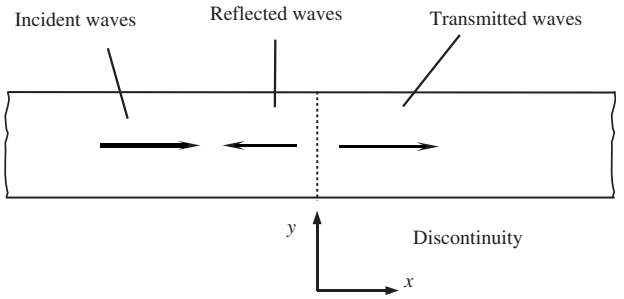

Fig. 2. Wave propagation with the discontinuity.

where W_1 and W_2 are the vertical deflections of sub-beams 1 and 2, respectively; E_1I_1 and E_2I_2 are the stiffness of sub-beams 1 and 2, respectively; and ρ_1A_1 and ρ_2A_2 are the masses per unit length of sub-beams 1 and 2, respectively.

Eq. (11) can be rewritten in spectral form by

$$\begin{aligned}&\frac{\partial^4\hat{W}_1}{\partial x^4}-k_1^4\hat{W}_1=0,\quad x\leqslant 0,\\&\frac{\partial^4\hat{W}_2}{\partial x^4}-k_2^4\hat{W}_2=0,\quad x\geqslant 0,\end{aligned}\tag{12}$$

where $k_1^4=\omega^2(\rho_1A_1/E_1I_1)$ and $k_2^4=\omega^2(\rho_2A_2/E_2I_2)$.

In this paper, two semi-infinite beams are considered. A complete solution of flexural displacement for sub-beams 1 and 2 is given by [14]

$$\begin{aligned}W_1(x,t)&=\int_0^\infty \hat{W}_1e^{i\omega t}\,d\omega=\int_0^\infty [Be^{-ik_1x}+Ce^{k_1x}+De^{ik_1x}]e^{i\omega t}\,d\omega,\\W_2(x,t)&=\int_0^\infty \hat{W}_2e^{i\omega t}\,d\omega=\int_0^\infty [Fe^{-ik_2x}+Ge^{-k_2x}]e^{i\omega t}\,d\omega,\end{aligned}\tag{13}$$

where ω is the frequency parameter; k_1 and k_2 represent the bending wavenumbers of sub-beams 1 and 2 related ω, respectively; waves in sub-beam 1 consist of an incident wave Be^{-ik_1x}, reflected wave De^{ik_1x} and reflected near-field wave Ce^{k_1x} (exponentially decaying with distance); and sub-beam 2 contains a transmitted wave Fe^{-ik_2x} and transmitted near-field wave Ge^{-k_2x}.

The coefficients C, D, F and G can be calculated by four continuity conditions at the discontinuity

$$\begin{aligned}&\textit{Displacement}:\ W_1=W_2,\\&\textit{Slope}:\ \frac{\partial W_1}{\partial x}=\frac{\partial W_2}{\partial x},\\&\textit{Moment}:\ E_1I_1\frac{\partial^2W_1}{\partial x^2}=E_2I_2\frac{\partial^2W_2}{\partial x^2},\\&\textit{Shear force}:\ E_1I_1\frac{\partial^3W_1}{\partial x^3}=E_2I_2\frac{\partial^3W_2}{\partial x^3}.\end{aligned}\tag{14}$$

According to Eq. (14), Eq. (13) can be written as

$$\begin{aligned}&B+C+D=F+G,\\&-ik_1B+k_1C+ik_1D=-ik_2F-k_2G,\\&E_1I_1\left(-k_1^2B+k_1^2C-k_1^2D\right)=E_2I_2\left(-k_2^2F+k_2^2G\right),\\&E_1I_1\left(ik_1^3B+k_1^3C-ik_1^3D\right)=E_2I_2\left(ik_2^3F-k_2^3G\right).\end{aligned}\tag{15}$$

Eq. (15) can be rewritten in matrix form by

$$\begin{pmatrix} 1 & 1 & -1 & -1 \\ 1 & \mathrm{i} & \mathrm{i}K & K \\ 1 & -1 & K^2\psi & -K^2\psi \\ 1 & -\mathrm{i} & -\mathrm{i}K^3\psi & K^3\psi \end{pmatrix} \begin{pmatrix} C \\ D \\ F \\ G \end{pmatrix} = \begin{pmatrix} -B \\ \mathrm{i}B \\ B \\ -\mathrm{i}B \end{pmatrix}, \tag{16}$$

where

$$K = \frac{k_2}{k_1} = \sqrt[4]{\frac{\rho_2 A_2}{E_2 I_2}\frac{E_1 I_1}{\rho_1 A_1}}$$

and

$$\psi = \frac{E_2 I_2}{E_1 I_1}.$$

Therefore, solving Eq. (16) in terms of B yields

$$\begin{pmatrix} C \\ D \\ F \\ G \end{pmatrix} = \begin{pmatrix} 1 & 1 & -1 & -1 \\ 1 & \mathrm{i} & \mathrm{i}K & K \\ 1 & -1 & K^2\psi & -K^2\psi \\ 1 & -\mathrm{i} & -\mathrm{i}K^3\psi & K^3\psi \end{pmatrix}^{-1} \begin{pmatrix} -1 \\ \mathrm{i} \\ 1 \\ -\mathrm{i} \end{pmatrix} B. \tag{17}$$

Further, these coefficients can be obtained by

$$\begin{pmatrix} \frac{C}{B} \\ \frac{D}{B} \\ \frac{F}{B} \\ \frac{G}{B} \end{pmatrix} = \begin{pmatrix} \dfrac{(1-K^4\psi^2)(1-i)}{(1+K^2\psi)^2+2K\psi(1+K^2)} \\ \dfrac{2K\psi(1-K^2)-i(1-K^2\psi)^2}{[(1+K^2\psi)^2+2K\psi(1+K^2)]} \\ \dfrac{2(1+K)(1+K^2\psi)}{K[(1+K^2\psi)^2+2K\psi(1+K^2)]} \\ \dfrac{2(K^2\psi-1)(1+\mathrm{i}K)}{K[(1+K^2\psi)^2+2K\psi(1+K^2)]} \end{pmatrix}. \tag{18}$$

It is noted that there is a sign error in transmission coefficients t_j (which characterizes the quasistationary motion behind the discontinuity) by Cremer et al. [14]. The transmission coefficient t_j should be

$$t_j = \frac{2(\hat{\psi}-1)-\mathrm{i}2\kappa(1-\hat{\psi})}{\kappa(1+\hat{\psi})^2+2\hat{\psi}(1+\kappa^2)},$$

rather than.

$$t_j = \frac{2(1-\hat{\psi})-\mathrm{i}2\kappa(1-\hat{\psi})}{\kappa(1+\hat{\psi})^2+2\hat{\psi}(1+\kappa^2)}.$$

Where $\kappa = K$ and $\hat{\psi} = K^2\psi$, two coefficients K and Ψ in Eq. (18) can be calculated if the parameters of this structure and its material properties ($\rho_1, A_1, E_1, I_1, \rho_2, A_2, E_2, I_2$) are known. Then the beam will behave in the same way. It is interesting to examine the effects of the beam thickness ratio $\gamma = h_2/h_1$ on these coefficients. In addition, this knowledge is useful to understand how the energy is reflected or transmitted at the discontinuity.

A full solution of an infinite beam with an initial disturbance imposed on it of the Gaussian waveform is introduced to further demonstrate the validity of the AWP technique. Generally, an incident Gaussian wave packet (a superposition of plane waves) is used to simulate the initial impulse or shock excitation. Its wave

function is given by

$$W(x,t)|_{t=0} = f_0 \mathrm{e}^{\left(-\frac{(x-x_0)^2}{4\sigma^2}\right)}, \quad \dot{W}(x,t)|_{t=0} = 0, \tag{19}$$

where $W(x, t)$ represents the deflection displacement of the beam in the z-direction; and f_0, x_0 and σ represent the maximum amplitude, the location of the peak of the initial wave packet and Gaussian factor, respectively. It is noted that σ determines the spatial spread of the wave packet and energy width.

The displacement of a single thin beam subject to a Gaussian excitation has the following analytical solution [15]:

$$W(x,t) = \frac{f_0}{(1+\tau^2)^{1/4}} \mathrm{e}^{\left(-\frac{\mu^2}{(1+\tau^2)}\right)} \times \cos\left(\frac{\mu^2\tau}{1+\tau^2} - \frac{1}{2}\tan^{-1}(\tau)\right), \tag{20}$$

where

$$\tau = \sqrt{\frac{EI}{\rho A}}\frac{t}{\sigma^2} \quad \text{and} \quad \mu = \frac{x}{2\sigma}.$$

When all the near-field terms are considered, the exact analytical solutions of the displacement of a stepped beam structure subject to a Gaussian distribution are given by

$$W_1(x,t) = \frac{f_0\sigma}{\left[\sigma^4 + \left(a_z^{(1)}t\right)^2\right]^{1/4}} \left[\mathrm{e}^{\left(-\frac{\sigma^2(x-x_0)^2}{4\left[\sigma^4+\left(a_z^{(1)}t\right)^2\right]}\right)} \times \cos\zeta^{(1)} + \frac{C}{B} \times \mathrm{e}^{\left(\frac{\sigma^2(x-x_0)^2}{4\left[\sigma^4+\left(a_z^{(1)}t\right)^2\right]}\right)} \times \cos\zeta^{(C)} + \frac{D}{B} \times \mathrm{e}^{\left(-\frac{\sigma^2(x+x_0)^2}{4\left[\sigma^4+\left(a_z^{(1)}t\right)^2\right]}\right)} \times \cos\zeta^{(2)} \right],$$

$$W_2(x,t) = \frac{f_0\sigma}{\left[\sigma^4 + \left(a_z^{(2)}t\right)^2\right]^{1/4}} \left[\frac{F}{B}\mathrm{e}^{\left(-\frac{\sigma^2(x-x_0)^2}{4\left[\sigma^4+\left(a_z^{(2)}t\right)^2\right]}\right)} \times \cos\zeta^{(3)} + \frac{G}{B} \times \mathrm{e}^{\left(\frac{\sigma^2(x-x_0)^2}{4\left[\sigma^4+\left(a_z^{(2)}t\right)^2\right]}\right)} \times \cos\zeta^{(G)} \right], \tag{21}$$

where $\zeta^{(1)} - \zeta^{(3)}$, $\zeta^{(C)}$, $\zeta^{(G)}$, $a_z^{(1)}$ and $a_z^{(2)}$ are given in Ref. [16].

Without the near-field terms, the approximate analytical solutions of the displacement for a stepped beam structure subject to a Gaussian distribution are given by

$$W_1(x,t) = \frac{f_0\sigma}{\left[\sigma^4 + \left(a_z^{(1)}t\right)^2\right]^{1/4}} \left[\mathrm{e}^{\left(-\frac{\sigma^2(x-x_0)^2}{4\left[\sigma^4+\left(a_z^{(1)}t\right)^2\right]}\right)} \times \cos\zeta^{(1)} + \frac{1-K}{1+K} \times \mathrm{e}^{\left(-\frac{\sigma^2(x+x_0)^2}{4\left[\sigma^4+\left(a_z^{(1)}t\right)^2\right]}\right)} \times \cos\zeta^{(2)} \right],$$

$$W_2(x,t) = \frac{2f_0\sigma}{1+K} \times \frac{\mathrm{e}^{\left(-\frac{\sigma^2(x-x_0)^2}{4\left[\sigma^4+\left(a_z^{(2)}t\right)^2\right]}\right)}}{\left[\sigma^4 + \left(a_z^{(2)}t\right)^2\right]^{1/4}} \times \cos\zeta^{(3)}. \tag{22}$$

For example, the bending moment and stress related to Eq. (22) can be calculated by

$$M(x,t) = -E(x)I(x)\frac{\partial^2 W(x,t)}{\partial x^2}, \quad \sigma_{\mathrm{Stress}}(x,t) = -\frac{E(x)h(x)}{2}\frac{\partial^2 W(x,t)}{\partial x^2}. \tag{23}$$

The bending moment and stress related to the full exact analytical solution given by Eq. (21) could also be calculated by using Eq. (23). It is noted that the stress has the same distribution as described in Eq. (23) but is different between the coefficients $I(x)$ for moment and $(h(x)/2)$ for stress.

2.4. Effects of near-field waves and beam thickness ratio on reflection and transmission coefficients, and transmission efficiencies

When the effect of near-field waves is considered, the coefficients in Eq. (18) are complex except for the third term F/B. Figs. 3 and 4 show the effect of the beam thickness ratio γ on the real part and imaginary parts of the coefficients with near-field terms, respectively. When $\gamma < 1$, that is, when waves are being transmitted from a large beam to a small beam, the value of the coefficient F/B increases. As γ increases, its magnitude greatly decreases. It is also noted that its value is exactly equal to 1 when $\gamma = 1$. In addition, the coefficient D/B is zero, as shown in Fig. 3. This means that the incident wave will fully transmit without any reflection when there is no step in the structure. As γ increases further, the coefficient F/B will gradually decrease to zero, whereas, the coefficient D/B will gradually increase with larger and larger phase change. This could be explained because there was no transmission if the end of the thin beam is attached to a very big mass. In this case, the incident wave will be totally reflected. As shown in Fig. 4, the imaginary part of this term is zero, which means the transmitted wave is always in phase with the incident wave, that is, both waves are travelling in the same direction.

However, the other coefficients may have a phase change. The coefficient D will have the same magnitude as that of the incident wave B, but with a negative phase change, as shown in Fig. 4. A reflection coefficient is a structural property, and does not depend on the incident wave amplitude in a linear system. There are many differences between the near-field terms C/B and G/B, as shown in Figs. 3 and 4. The real parts of the coefficient C/B and the coefficient F/B have similar relationships with the beam thickness ratio γ, apart from a difference in magnitude. When $\gamma < 1$, the two coefficients C/B and G/B have great changes in both magnitudes and phase, as shown in Figs. 3 and 4. It is worth noting that the real and imaginary parts of the two evanescent coefficients are zero when $\gamma = 1$. Furthermore, as γ increases, the coefficient G/B (both the real and imaginary parts) will slowly tend towards zero.

According to the definition provided by Cremer et al. [14], the transmission efficiency τ (the ratio of transmitted to incident power) can be calculated by

$$\tau = \frac{4K\psi(1+K)^2(1+K^2\psi)^2}{[(1+K^2\psi)^2 + 2K\psi(1+K^2)]^2}. \tag{24}$$

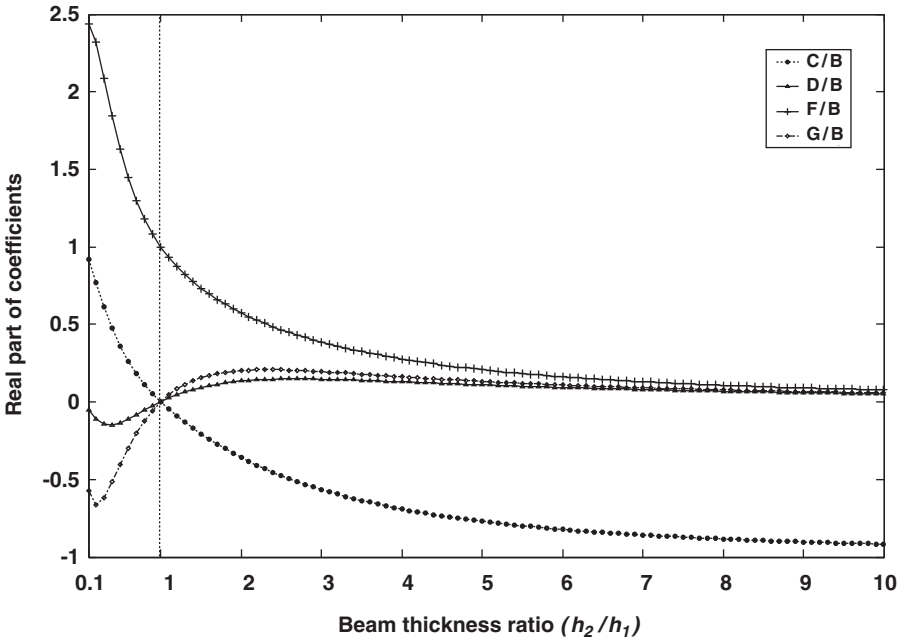

Fig. 3. Effect of the beam thickness ratio on the real part of the transmission and evanescent coefficients.

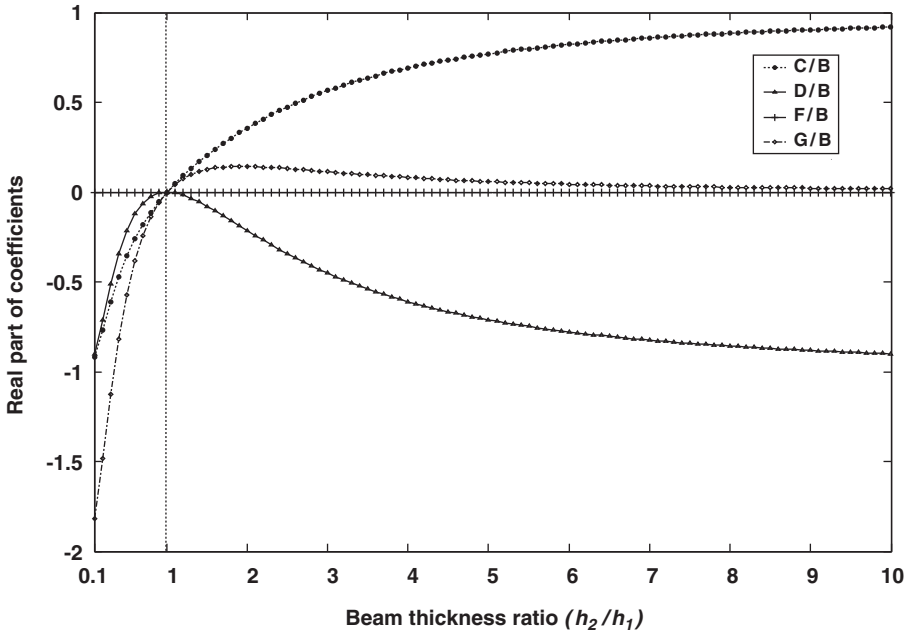

Fig. 4. Effect of the beam thickness ratio on the imaginary part of the transmission and evanescent coefficients.

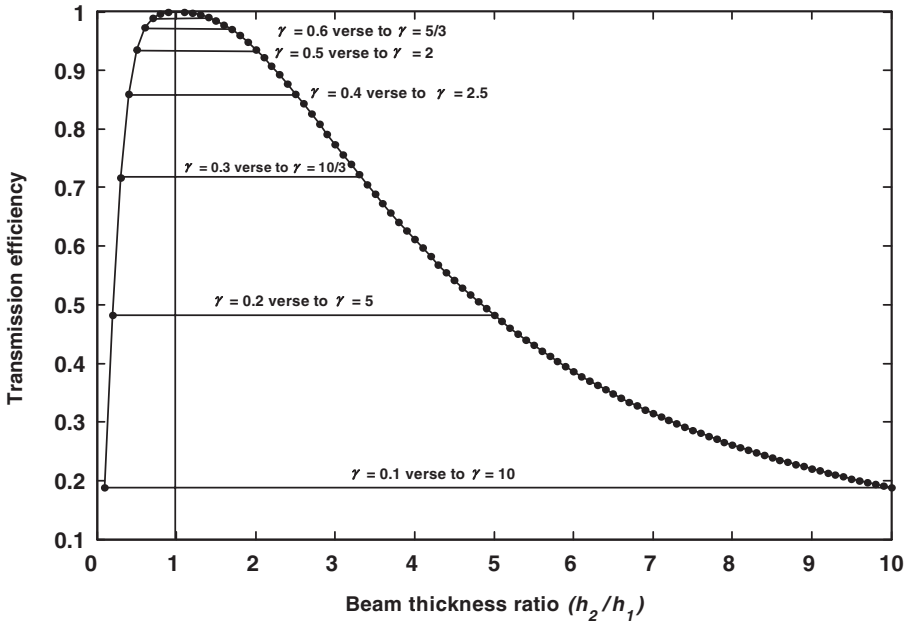

Fig. 5. Transmission efficiency across a stepped beam discontinuity as function of beam thickness ratio.

Fig. 5 shows how the transmission efficiency τ varies with the beam thickness ratio γ. Around $\gamma = 1$ marked by the vertical dotted line, a small difference in thickness does not affect the transmission of bending waves appreciably. However, large changes in thickness result in significant effects, as shown in Fig. 5. It is noted that the transmission efficiency τ has the same value when $\gamma = 0.1$ and 10; $\gamma = 0.2$ and 5; $\gamma = 0.3$ and $10/3$; $\gamma = 0.4$ and 2.5, and so on. This demonstrates that the transmission efficiency τ will be constant if the beam

thickness ratio γ is given. In other words, the transmission efficiency τ from a thin beam to a thick beam is the same as that from the thick beam to the thin beam, for a given stepped beam.

The following derivation further verifies this conclusion:

$$\tau(1/\gamma) = \tau\left(\frac{h_1}{h_2}\right) = \frac{\frac{4}{K\psi}\left(1+\frac{1}{K}\right)^2\left(1+\frac{1}{K^2\psi}\right)^2}{\left[\left(1+\frac{1}{K^2\psi}\right)^2+\frac{2}{K\psi}\left(1+\frac{1}{K^2}\right)\right]^2} = \frac{4K\psi(1+K)^2(1+K^2\psi)^2}{[(1+K^2\psi)^2+2K\psi(1+K^2)]^2}$$
$$= \tau(\gamma) = \tau\left(\frac{h_2}{h_1}\right). \tag{25}$$

For example, $\tau(0.1) = \tau(10) = 0.1883$, $\tau(0.2) = \tau(5) = 0.4823$ and $\tau(0.3) = \tau(10/3) = 0.7169$.

2.5. Transient energy flow in a one-dimensional stepped beam structure

The knowledge of transient energy flow and transmission and reflection coefficients in beams with a sudden change in cross-section is important in engineering design and other practical applications. Many techniques are presented in the literature that investigates energy flow and transmission and reflection coefficients. Power flow analysis (PFA) and statistical energy analysis (SEA) have become widely accepted as useful techniques for predicting statistical responses of dynamic systems and vibrational energy flow passing through structures in the frequency domain [17–21]. However, only a few theoretical expressions are available for estimating the energy flow and coupling loss factors for complex structures in the time domain. It is therefore necessary to develop an accurate and efficient method to predict the distribution of energy flow and determine the dominant paths of energy flow through the structure, in particular, reflection and transmission around discontinuities. This section extends the AWP technique to investigate energy flow in a one-dimensional structure with a discontinuity. The AWP technique provides a time-domain method to accurately predict energy flow and coupling loss in complex coupled structures. This analysis also supplies a theoretical framework that can be used to experimentally measure energy flow and energy loss in beams at the location of a sudden change in cross-section.

The general analytical solutions of displacement of the above structure are given in the time domain (Eqs. (13) and (18)). Equations for the intensity I in beams usually indicate the distribution of the energy flow or power, because they typically use the total flexural stiffness EI of the beam. In addition, the definition of the intensity I in beams is a little different from that in plates, which usually gives the energy flow per unit width, because it typically utilizes the flexural stiffness per unit width of the plate. The x components of the intensities for sub-beams 1 and 2 are made up of the force contribution and the bending moments' contributions. In the time domain, the energy intensity with exact analytical solutions of a stepped beam can be calculated by

$$I_x^{(1)} = \left(M_1\frac{\partial}{\partial t}\left(\frac{\partial W_1}{\partial x}\right) + Q_1\frac{\partial W_1}{\partial t}\right),$$
$$I_x^{(2)} = \left(M_2\frac{\partial}{\partial t}\left(\frac{\partial W_2}{\partial x}\right) + Q_2\frac{\partial W_2}{\partial t}\right). \tag{26}$$

The structural intensity given by Eq. (26) is also obtained for the case of a stepped beam subject to a Gaussian distribution, by using the exact analytical solution of the displacement given by Eq. (21). The various terms

$$\frac{\partial}{\partial t}\left(\frac{\partial W_1}{\partial x}\right) = \frac{\partial}{\partial x}\left(\frac{\partial W_1}{\partial t}\right) = \frac{\partial V_1}{\partial x},\ \frac{\partial W_1}{\partial t},\ \frac{\partial W_2}{\partial t},\ \frac{\partial V_2}{\partial t}$$

can be obtained by the derivatives of Eq. (21) with respect to time t and spatial variable x. More details can be found in Ref. [16]. The predicted results obtained by the AWP technique can be compared with those analytical solutions to examine its accuracy and efficiency.

3. Numerical analysis and discussions

For simplicity, the two sub-beams are assumed to be made of the same materials. Their material properties are $E = 21.6 \times 10^{10}\,\mathrm{N/m^2}$, and $\rho = 7800\,\mathrm{kg/m^3}$. The parameters of the beams are $x_L = 10\,\mathrm{m}$, $h_1 = 0.002\,\mathrm{m}$, $h_2 = 0.005\,\mathrm{m}$, $A_1 = 4 \times 10^{-5}\,\mathrm{m^2}$ and $A_2 = 1 \times 10^{-4}\,\mathrm{m^2}$. The initial displacement and discontinuity are located at $x_0 = -1\,\mathrm{m}$ and $x_d = 0\,\mathrm{m}$, respectively.

In this simulation, the time step in the Chebyshev–Fourier scheme is $\mathrm{d}t_{\mathrm{Ch}} = 0.0001\,\mathrm{s}$. Sixty terms of Chebyshev polynomials are used in the expansion. The following initial state vector is chosen to demonstrate the application of the AWP

$$\Phi(x,0) = \begin{bmatrix} 0 \\ M(x,0) \end{bmatrix}, \tag{27}$$

where $M(x,0)$ is related to the initial displacement $W(x,0) = f_0 \mathrm{e}^{-((x-x_0)^2/4\sigma^2)}$. Other simulated parameters are given as follows: $f_0 = 0.001\,\mathrm{m}$, $\sigma = 0.1$, and the number of grid points N is 100. The spatial sampling interval Δx is 0.1 m. The evolution of wave packet and reflected waves is observed with $-6\,\mathrm{m} \leqslant x \leqslant 4\,\mathrm{m}$.

For a sharp discontinuity, this thickness discontinuity will pose the numerical difficulty of calculating the moments and stress terms. To assure numerical convergence, a boundary-smoothing technique was introduced by using the convolution with a Gaussian function $G(x)$

$$\bar{h}(x) = \frac{1}{2\pi} \int h(\tau) G(\tau) \mathrm{e}^{-\mathrm{i}x\tau} \mathrm{d}\tau = F^{-1}\left\{ F[h(x)] F\left[\mathrm{e}^{-((\xi - x)^2/\sigma^2)} \right] \right\}, \tag{28}$$

where σ denotes a Gaussian factor. It is critical to choose a suitable grid size N and σ to meet the demands of numerical convergence and computational efficiency. More details of the effect of grid size N and σ on numerical convergence and computational efficiency are discussed in Ref. [9].

3.1. Comparison of the predicted results between the Chebyshev–Fourier scheme and exact analytical solutions

Fig. 6 presents the displacement error (unit: mm) between the results predicted by the AWP technique and the exact analytical solution at $t = 0.034\,\mathrm{s}$ for $\gamma = 1$ (without the stepped discontinuity). It is found that the AWP technique is highly accurate and computationally effective due to the wave packet evolution with large time steps. Furthermore, Fig. 7 shows the comparison of the displacement predicted by the Chebyshev–Fourier scheme with the exact analytical solution for $\gamma = 2.5$ at different instants. At $t = 0.007\,\mathrm{s}$, the incident waves reach the discontinuity, which result in reflected waves. The absolute error of the displacement (unit: mm) is in the order of 10^{-5}. As time increases, more incident waves result in reflected waves, and more waves propagate into sub-beam 2 by passing through the discontinuity. As shown in Fig. 7(b), the two curves still agree very well. At $t = 0.034\,\mathrm{s}$, the effect of the introduced boundary-smoothing technique can be seen in Fig. 7(c). The error analysis of the AWP method has been undertaken in details in a published paper (Ref. [9]). It has been found that the error is controlled by the shapes and numbers of grids of the smooth and continuous curves in replacing the original discontinuities in the system parameters.

3.2. Wave propagation and stress distribution

Fig. 8 shows the evolution of the displacement $W(x, t)$ at different instants by the AWP technique. The discontinuity is located at $x_d = 0\,\mathrm{m}$, as shown in Fig. 1. The initial displacement with a Gaussian distribution is shown in Fig. 8(a). As time increases, the wave packets spread out to the two ends with decreased magnitudes. At $t = 0.007\,\mathrm{s}$, the wave reaches the discontinuity, which results in reflected waves. Due to the effect of reflected waves, the transmitted waves in sub-beam 2 continue to propagate with smaller magnitudes than those in sub-beam 1. The displacements with larger values exist from –2 to 0 m, as shown in Fig. 8(f).

Fig. 9 shows the distribution of the stress σ at different instants. An initial stress is illustrated in Fig. 9(a). The difference is that the transmitted waves at sub-beam 2 have larger magnitudes than those at sub-beam 1. As time increases, the magnitudes decay slowly, as shown in Figs. 9(e) and (f). It is noted that the effect of reflected wave on the stress is limited to near-fields (from -2 to 0 m) at sub-beam 1 because the reflected wave

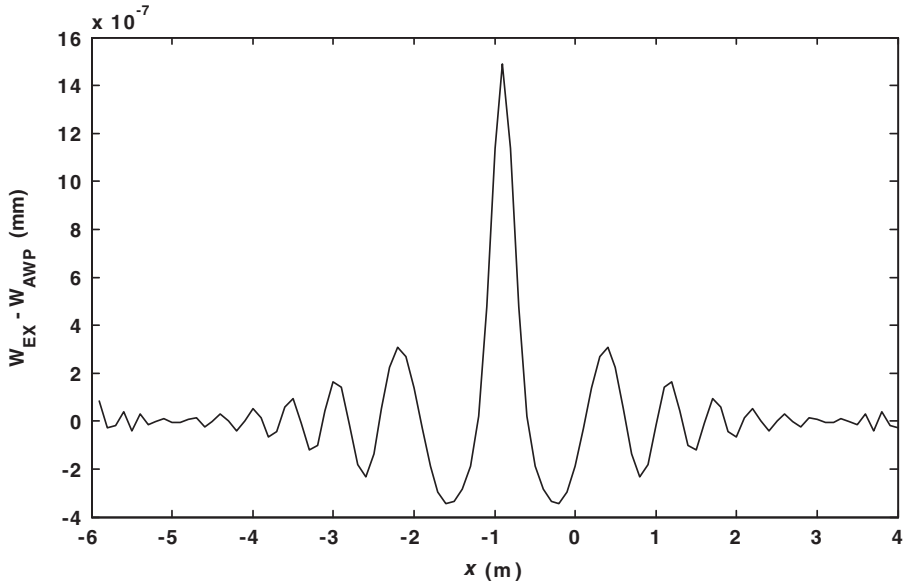

Fig. 6. Displacement error between the results predicted by the AWP technique and the exact analytical solution when $\gamma = 1$ and $t = 0.034$ s.

has not yet reached the far-field regions. The total stress is simply the sums of the stresses due to he individual waves, so the reflected wave will influence the stress levels when it reaches the far-field region. However, this influence maybe small if the reflection coefficient is small and/or damping is large, but it will be present. The magnitudes of the stress in sub-beams 1 and 2 are shown in Figs. 9(d)–(f).

Fig. 10 shows energy intensities in a stepped beam structure at different instants. A zero initial energy intensity including both moment and shear terms is illustrated in Fig. 10(a). The reason for the zero initial energy intensity is that the initial velocity is zero. As time increases, the moment term has a different distribution from the shear force term, as shown in Figs. 10(b)–(f). The total energy intensity is a combination of the moment term $M(\partial V/\partial x)$ and shear force term $F(\partial W/\partial t)$. One observation is that total energy intensities are dominated by the moment term near the discontinuity, and the shear force term away from the discontinuity before waves pass the discontinuity or just pass through the discontinuity, as shown in Figs. 10(b) and (c). As time further increases, waves propagate within the whole structure.

Effects of the moment term $M(\partial V/\partial x)$ and shear force term $F(\partial W/\partial t)$ on total energy intensities are totally different. In other words, total energy intensities are dominant by the shear force term near the discontinuity, and the moment term for the rest, as shown in Figs. 10(e) and (f). This observation cannot be explained by only considering distributions of the bending moment and shear force. In addition, distributions of the term $\partial V/\partial x$ (derivative of velocity with x) and velocity V should be considered to investigate the effect of the moment term $M(\partial V/\partial x)$ and shear force term $F(\partial W/\partial t)$ on energy intensity or energy flow. Another interesting observation is that the magnitude of energy intensity in Fig. 10(d) is much higher than those in other figures. One explanation is that, at this instant, both the moment term and shear force term have the biggest magnitudes when waves with the maximum magnitude pass through the discontinuity. It is noted that the remaining distributions (excluding the maximum value in Fig. 10(d)) have much lower magnitudes compared with those at other instants, as shown in Figs. 10(b), (c), (e) and (f). To further explain the above observation, distributions of the bending moment M and the angular velocity $\partial V/\partial x$ are shown in Figs. 11 and 12, respectively. Both the bending moment and angular velocity with large amplitudes are found near the discontinuity (far away to $x = -2$ m), as shown in Figs. 11 and 12. Therefore, for this case, the reflective wave is in phase with the incident wave during the scattering period, as a result the corresponding intensity has larger value close to the discontinuity. Although the angular velocity has larger amplitude further away from

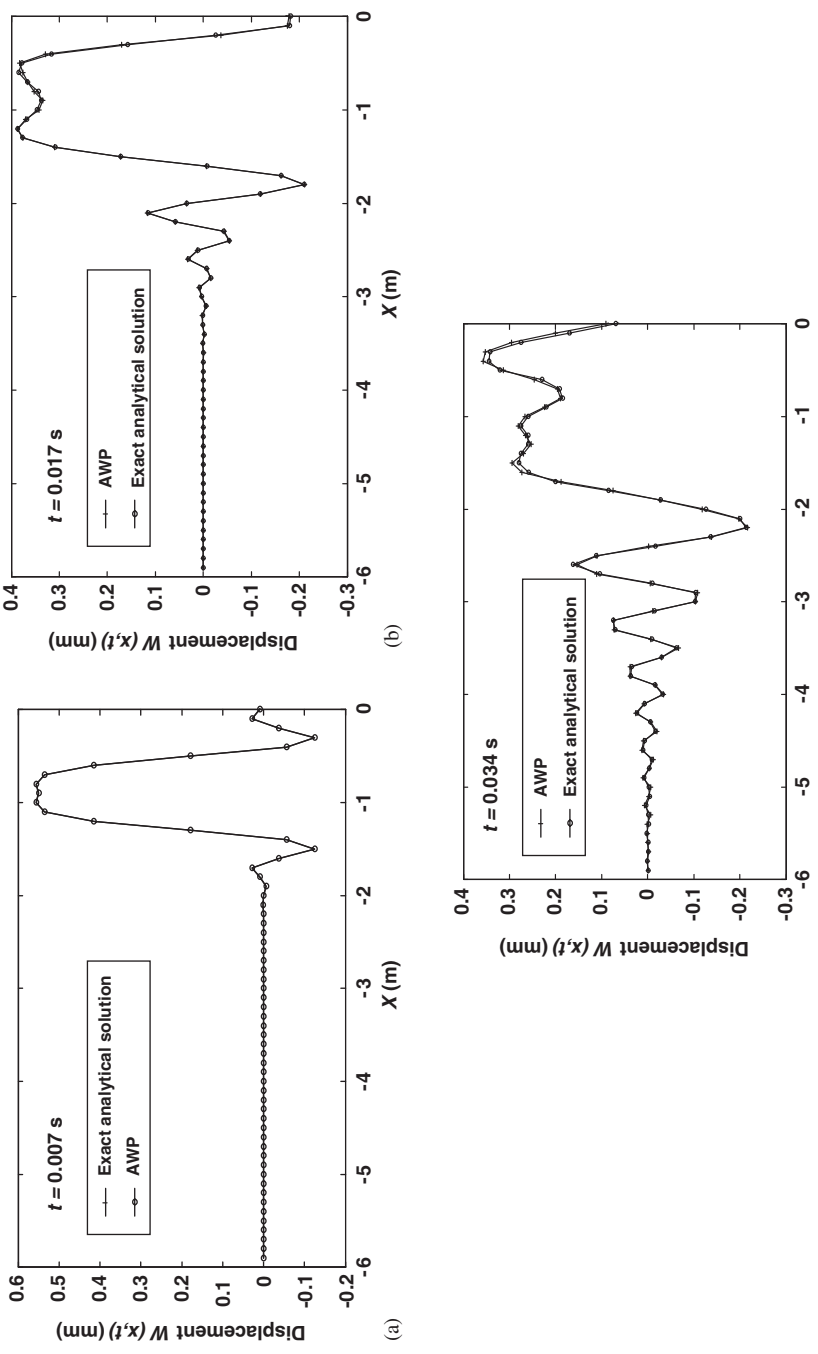

Fig. 7. Comparison of the results predicted by the AWP technique and those obtained with exact analytical solutions for $\gamma = 2.5$ at different instants.

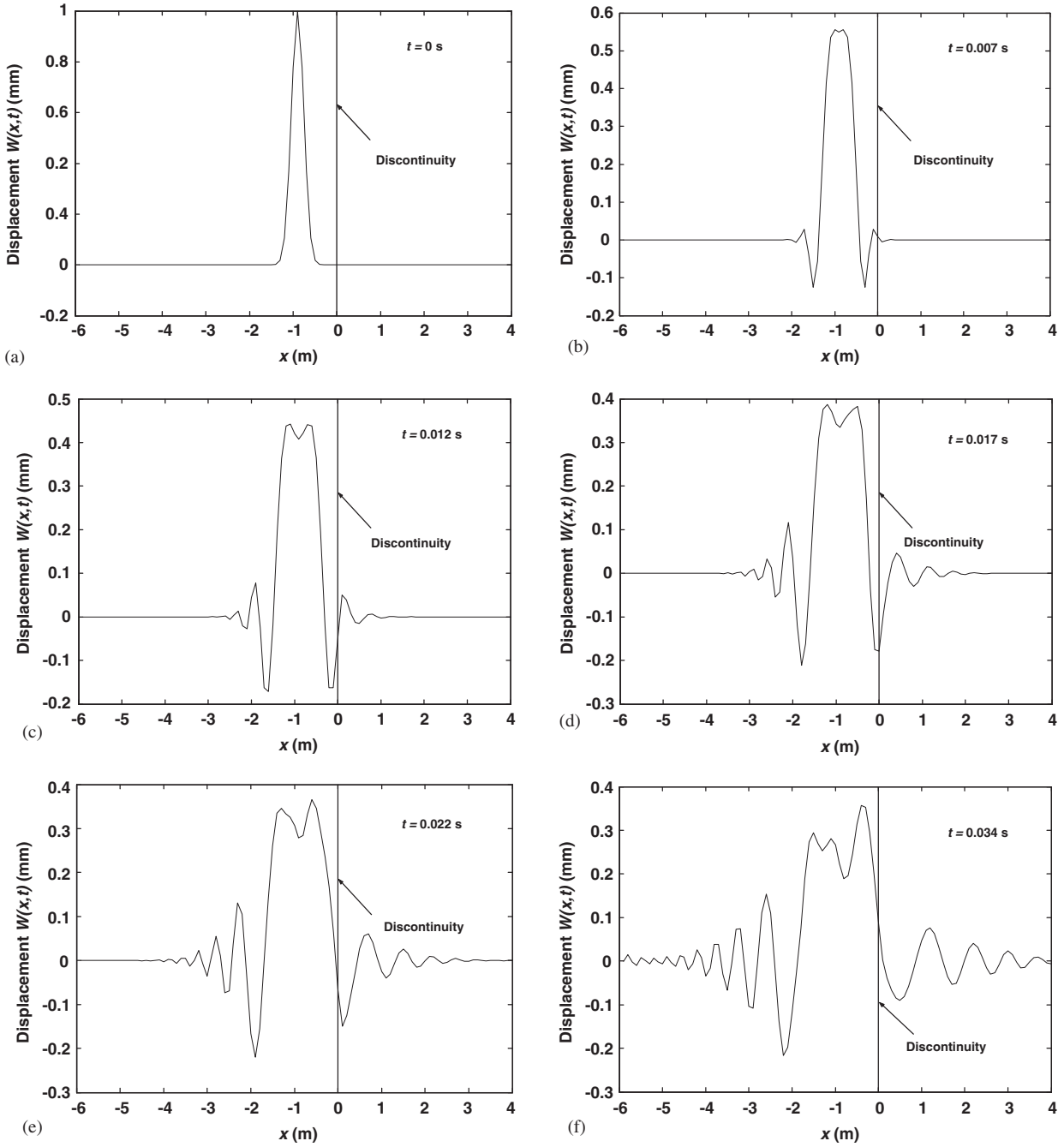

Fig. 8. The predicted results of the displacement $W(x, t)$ at different instants.

the discontinuity ($x = -5$ to -2 m) after $t = 0.017$ s, the reflected waves of bending moments have much smaller amplitudes. Thus, their products of the bending moment and angular velocity still have smaller values. Similarly, distributions of the shear force F and velocity V can be done to support the above observation in Fig. 10: the shear component dominate further away from the discontinuity. The above analysis is very helpful to get a good understanding of vibration characteristics of structures.

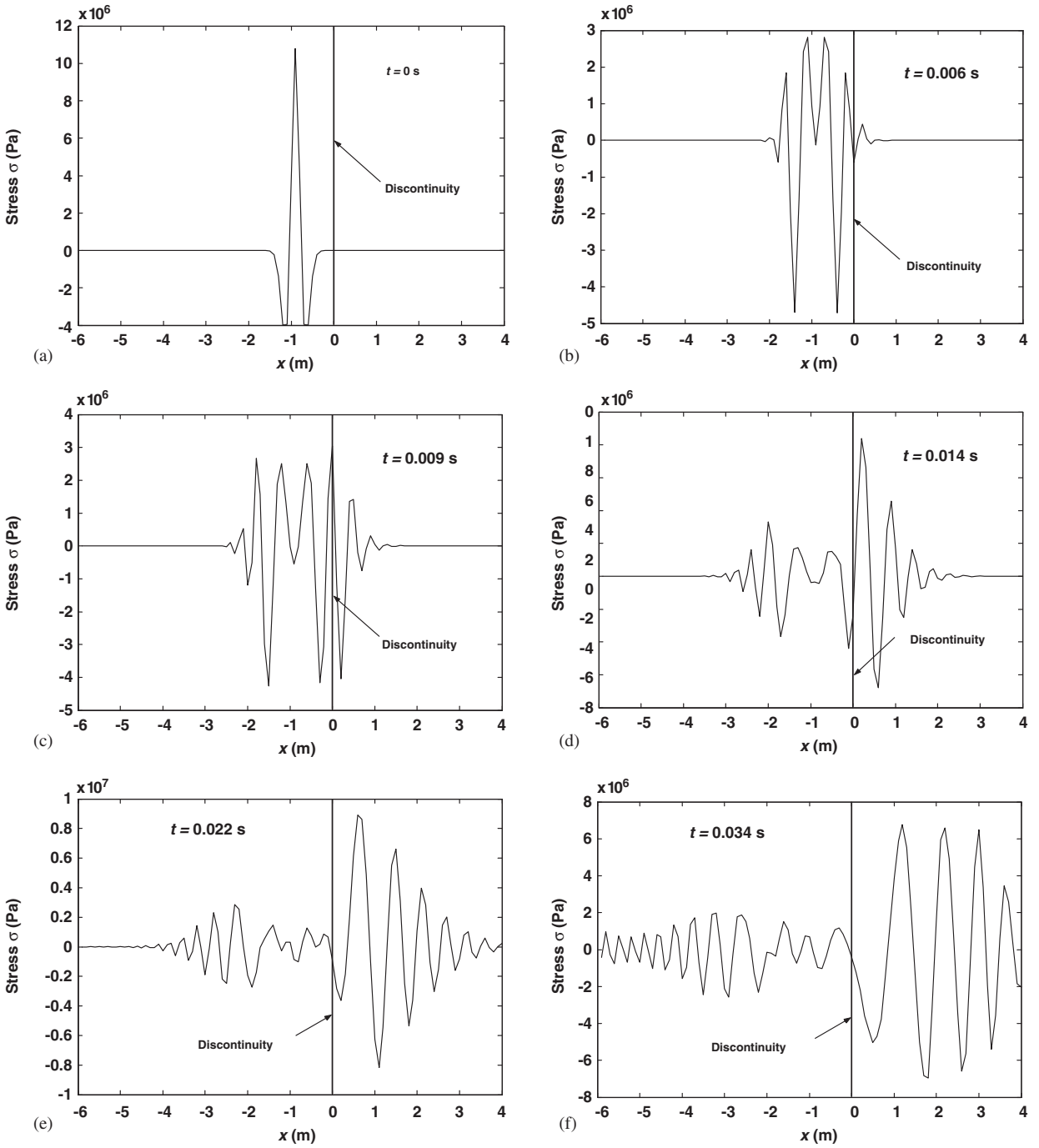

Fig. 9. The predicted results of the stress σ at different instants.

3.3. Experimental analysis of a stepped beam structure

An experimental analysis is carried out to investigate the reflection and transmission of bending waves at a discontinuity in cross-section in a stepped beam structure. The experimental results are presented here and compared with theoretical predictions. Through this kind of comparison, the validity of theoretical prediction as described in previous sections can be verified. Measurements of bending pulses were made on a stepped

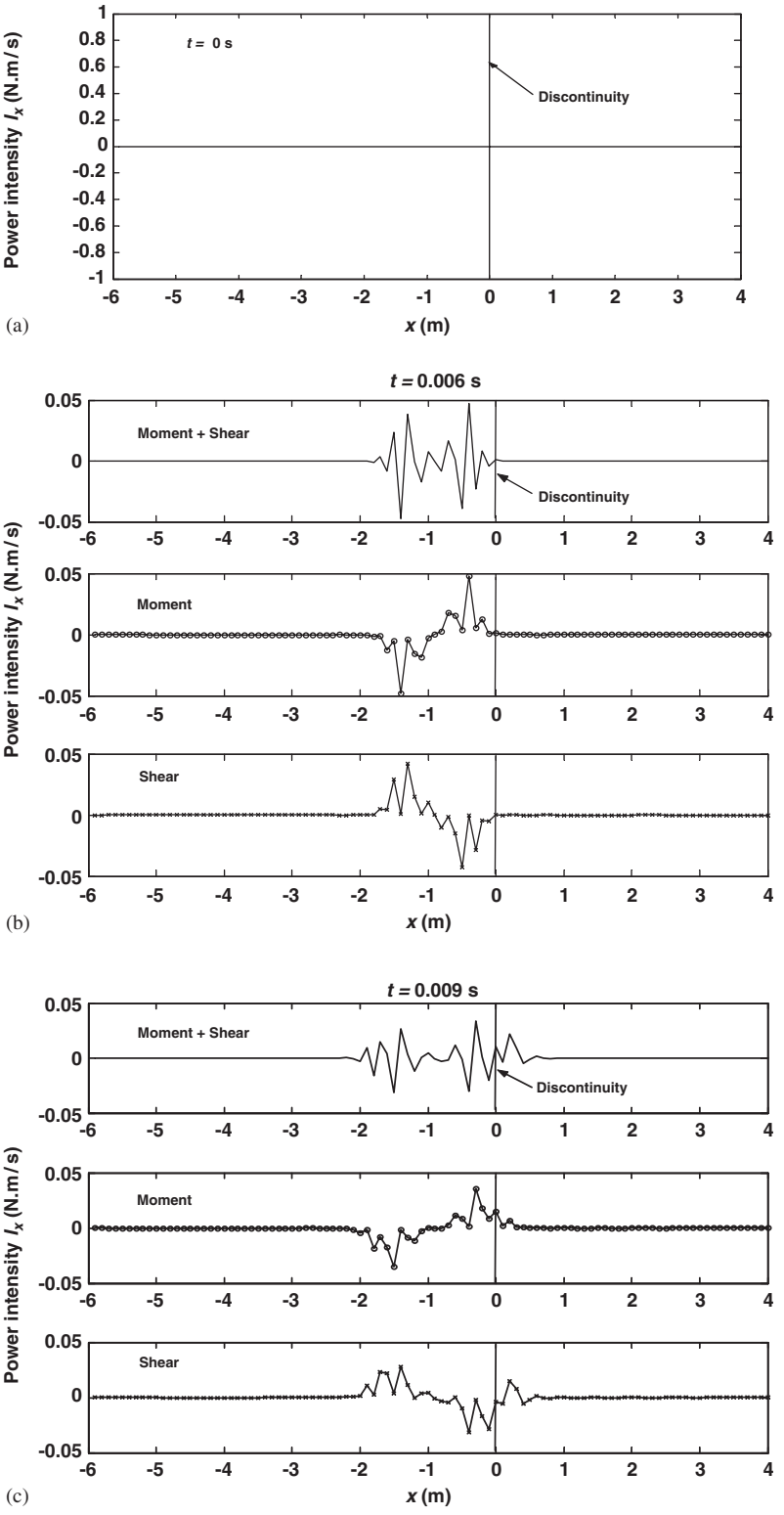

Fig. 10. Energy intensity at different instants.

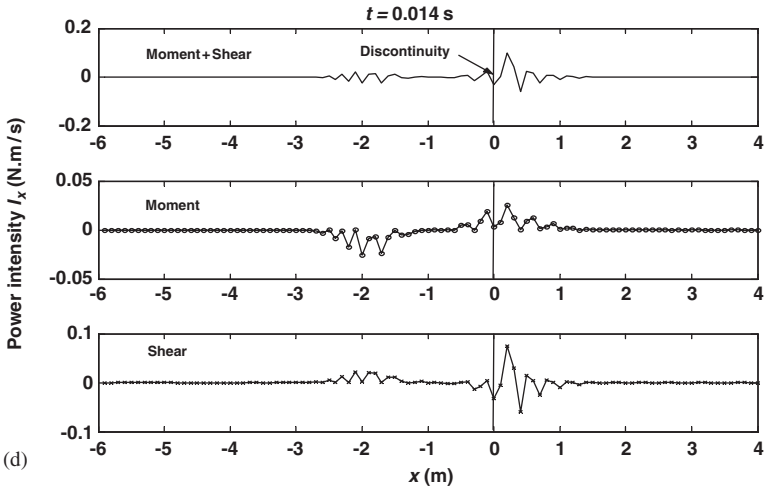

(d)

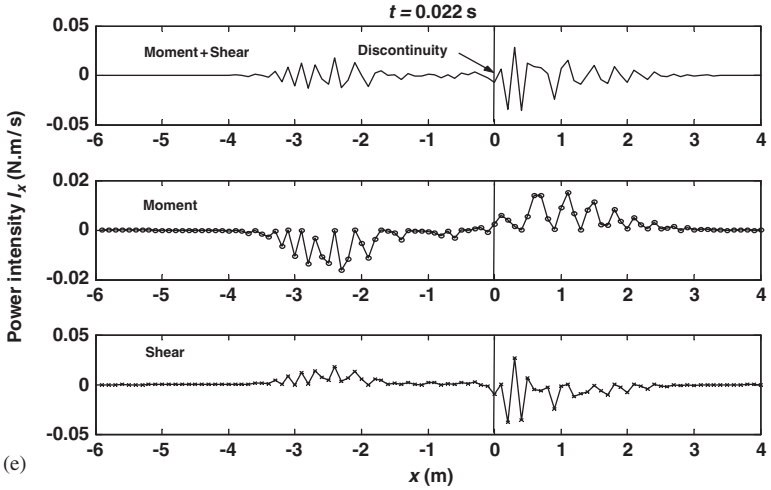

(e)

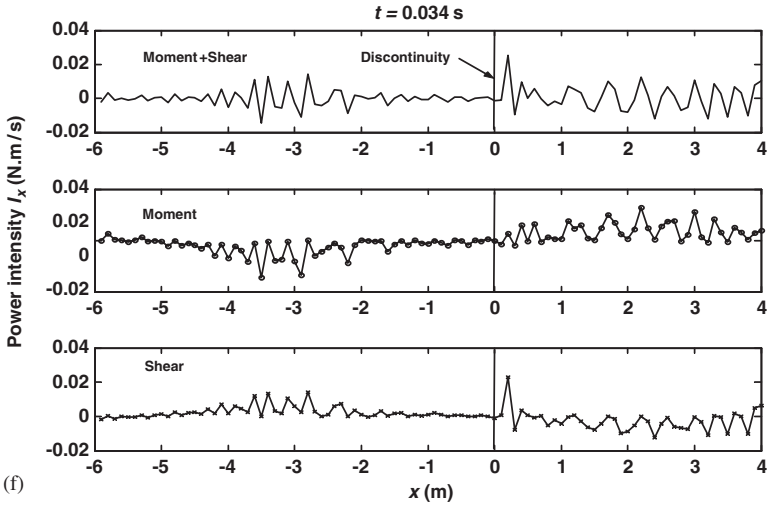

(f)

Fig. 10. (*Continued*)

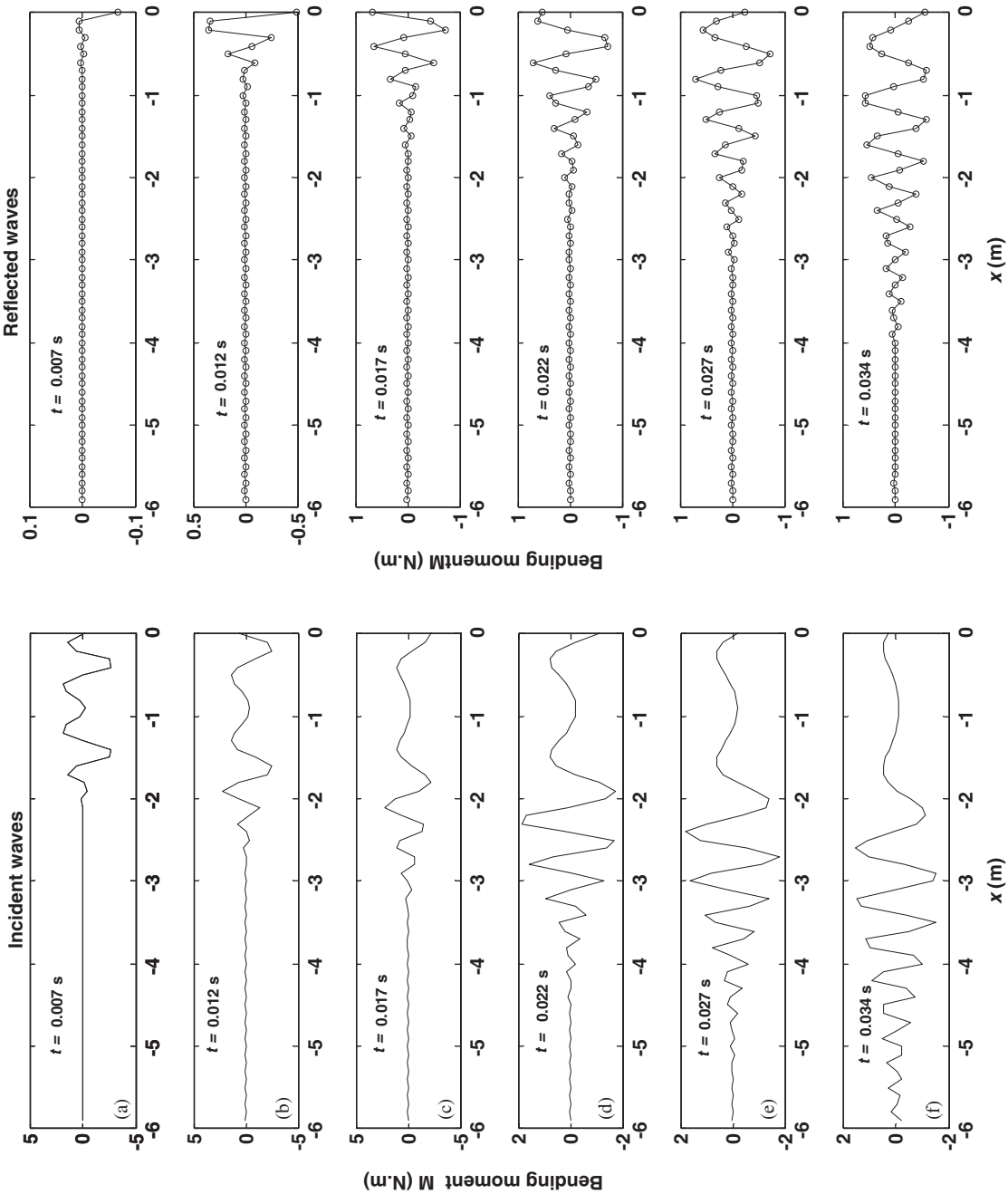

Fig. 11. Incident wave and reflected wave distributions of bending moments $M(x, t)$ at different instants.

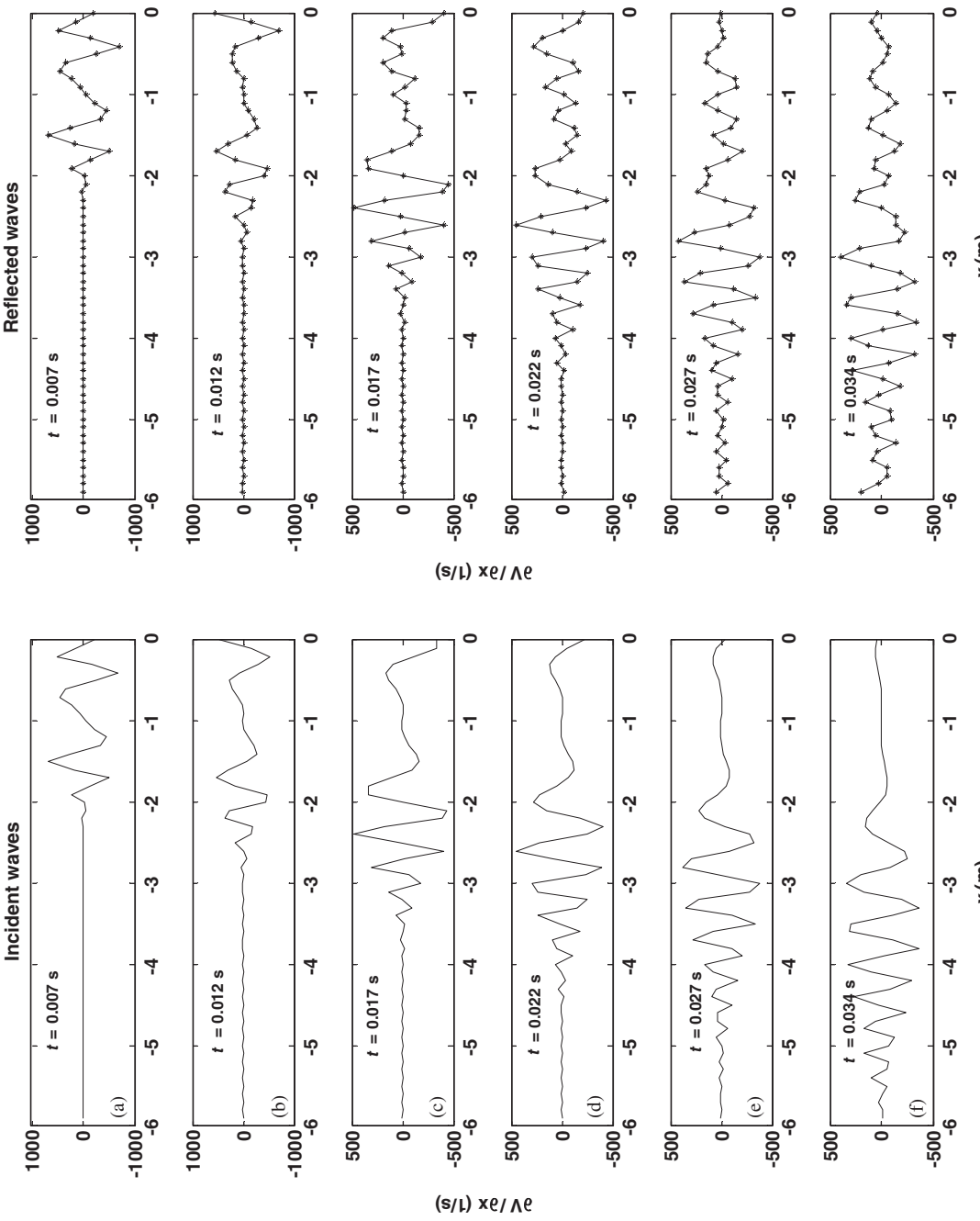

Fig. 12. Incident wave and reflected wave distributions of angular velocity $\partial V(x,t)/\partial x$ at different instants.

beam by using accelerometers and strain gauges. As shown in Fig. 13, a stepped beam is used in the experiment. The stepped beam is made of steel. The cross-sections of smaller beam and larger beam are, respectively, 10 mm × 6 mm with length of 100 mm, and 25 mm × 6 mm with length 400 mm (. The distances from points A, B and C to the end of smaller beam are 10 mm, 50 mm and 130 mm, respectively. One end of the beam is wrapped with soft material and buried in a box with soft sand (dimensions with length, width and height are 300 × 200 × 250 mm), which will provide an effective absorption for all wave types. To increase the structural stability and holding strength of the sand box, an extra holder at the end of the larger beam is specially designed and immersed in this sand box. The above experimental technology is usually used to simulate a semi-infinite beam. The other end of the smaller beam is supported by a fine steel wire. To clearly record the incident, the reflected and the transmitted pulses from a single impact, a small steel ball (4 mm diameter) fired from a spring-powered gun is used to strike the centre of one end of this structure. This instrument provides the consistent impact force during the whole measurement. For bending waves, the impact position is chosen as close to the end of the smaller beam as possible to produce flexible bending motions, as shown in Fig. 13. Travelling along the beam, the wave continually changes its amplitude and shape due to damping losses and wave dispersion. If these changes are negligible, the wave will propagate with a constant amplitude and shape. It is noted that the experimental investigation is carried out to study the flexible wave propagation, reflection and transmission from smaller beam cross-section to larger cross-section. Through another experimental set-up (smaller beam is buried in the sand box and larger beam is hung by a fine steel wire), the similar analysis can be carried out to investigate flexible wave propagation, reflection and transmission from larger beam cross-section to smaller cross-section, and hence the effect of a discontinuity on the wave propagation.

Accelerometers are often preferred due to their reusability, ease of installation, wide band frequency and dynamic response. Two accelerometers are mounted on sub-beam 1 and sub-beam 2, as shown in Fig. 13. One accelerometer is used to record the incident and reflected pulses. The other is used to record the transmitted pulse. To increase measured accuracy and efficiency, a multi-channel data acquisition system with Waveview software and de-noising technique is used to record the incident, the reflected and the transmitted pulses for a single impact.

The recording window is adjusted as so that only the incident and reflected waves from the change in cross-section appear on the scope screen. From the whole record, it is found that the reflection from the end in the sand box can be neglected. As mentioned above, the measured variable (acceleration, velocity and displacement) is primarily related to motion and gives only indirect information about stress within the material. Strain gauges, on the other hand, are preferably applied for low-frequency and medium-dynamic measurements. In making measurements, the strain gauges are properly connected with a specific amplifier circuit for measuring symmetrical strains. Then the small end of the beam is struck at its centre, and the incident, reflected, and transmitted pulses are measured.

Since the experimental results, which will be compared with the predicted results, are based on measurements of strain, which are proportional to moment, it is necessary to see how reflection and transmission coefficients for displacement are related to the corresponding quantities for moment. It is easily shown that

$$M_1(x,t) = E_1 I_1 (k_1)^2 \left[B e^{-ik_1 x} - C e^{k_1 x} + D e^{ik_1 x}\right] e^{i\omega t},$$
$$M_2(x,t) = E_2 I_2 (k_2)^2 \left[F e^{-ik_2 x} - G e^{-k_2 x}\right] e^{i\omega t}. \tag{29}$$

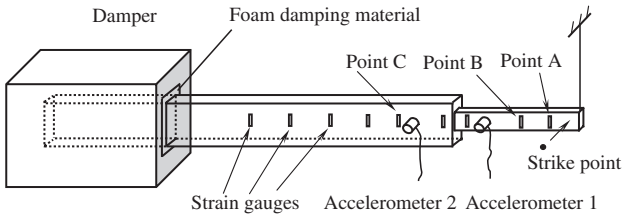

Fig. 13. Experimental set-up for a stepped beam structure.

D/B represents the amplitude ratio of the reflected moment relative to the incident moment, which is only true in the absence of near-fields. Here, if the contributions of the reflected and near-field waves are ignored, then Eq. (29) can be rewritten as

$$\begin{aligned} M_1(x,t) &= E_1 I_1 (k_1)^2 \left[B \mathrm{e}^{-\mathrm{i}k_1 x} \right] \mathrm{e}^{\mathrm{i}\omega t}, \\ M_2(x,t) &= E_2 I_2 (k_2)^2 \left[F \mathrm{e}^{-\mathrm{i}k_2 x} \right] \mathrm{e}^{\mathrm{i}\omega t}. \end{aligned} \tag{30}$$

Thus, the ratio of the transmitted moment to the incident moment is

$$\frac{E_2 I_2 (k_2)^2 F}{E_1 I_1 (k_1)^2 B} = K^2 \psi \frac{F}{B}. \tag{31}$$

The maximum strain often happen on the surfaces of the structure, thus they are given by

$$\varepsilon_{\max}^{(1)} = \pm \frac{h_1}{2} \frac{\partial^2 W_1}{\partial x^2}, \quad \varepsilon_{\max}^{(2)} = \pm \frac{h_2}{2} \frac{\partial^2 W_2}{\partial x^2}. \tag{32}$$

Therefore, they can be rewritten as

$$\frac{\varepsilon_{\max}^{(2)}}{\varepsilon_{\max}^{(1)}} = \frac{h_2 (\partial^2 W_2 / \partial x^2)}{h_1 (\partial^2 W_1 / \partial x^2)} = \frac{h_2 M_2}{h_1 \psi M_1} = \frac{h_2 K^2}{h_1} \frac{F}{B}. \tag{33}$$

As shown in Eq. (29), the ratio M_2/M_1 involves wave amplitudes B, C, D, F and G. Here, only two dominate wave amplitudes B and F are considered in Eq. (31) to compare with the ratio of measured strains. In other words, these omitted terms can be assumed zero with safety due to "gating" of the signal or distance from the discontinuity. Hence F/B multiplied by the constant

$$\frac{h_2}{h_1} \sqrt{\frac{\rho_2 A_2 E_1 I_1}{\rho_1 A_1 E_2 I_2}},$$

when the structural materials are known, represents the ratio of the amplitude of the transmitted bending strain to the amplitude of the incident strain, and comparisons of amplitudes can be directly made from the strain measurements. For a special case, the stepped beam is made of the same material, thus Eq. (33) can be simplified into $\varepsilon_{\max}^{(2)}/\varepsilon_{\max}^{(1)} = F/B$, which means the ratio of the amplitude of the transmitted bending strain to the amplitude of the incident strain can be directly obtained from the strain measurements.

Fig. 14 shows the effect of beam thickness ratio on the ratio of the amplitude of the transmitted bending strain in sub-beam 2 to that of the incident strain in sub-beam 1. For a special case $\gamma = 1$ (uniform beam without any step), the strain ratio is 1 providing that light material damping and energy radiation into air are neglected, as shown in Fig. 14. For a pair of beams having a thickness ratio of $\gamma = 2.5$, the strain ratio and theoretical predictions for reflection and transmission coefficients (propagating from the small end toward the large end) are

$$\gamma_{\text{Stress}} = 0.5, \ \left| \frac{D}{B} \right| = 0.19, \ \left| \frac{F}{B} \right| = 0.59. \tag{34}$$

Fig. 15 shows experimental results for flexural waves at three measured points A, B, and C on the stepped beam structure, as shown in Fig. 13. Fig. 15(b) has the similar pattern as Fig. 15(a) except for a little difference in magnitude. Qualitatively, if we neglect material damping, energy radiation into air and the effects of dispersion, the result at point B should have the similar distribution as that at point A. It is noted that point B will differ from point A not only by a time delay (propagating time from point A to point B), but also in the magnitude and phase due to the dispersive system. Experimental results in Figs. 15(a) and (b) also support the above analysis. Due to the discontinuity, reflection waves can be clearly seen in both Fig. 15(a) and Fig. 15(b). It is worth noting that the experimental results in Fig. 15 were obtained under the same impact. In other words, with multi-channel measuring systems, the results of points A, B and C can be simultaneously obtained. Therefore, Fig. 15 shows the measured results normalized by the magnitude of the first positive peak of experimental result at measuring point A.

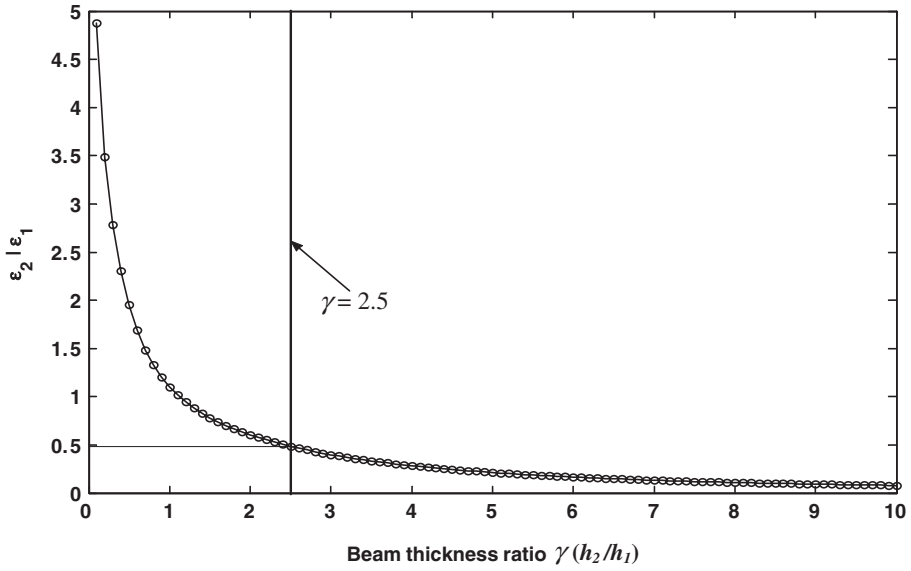

Fig. 14. Ratio of the transmitted bending strain to the incident strain as a function of the beam thickness ratio.

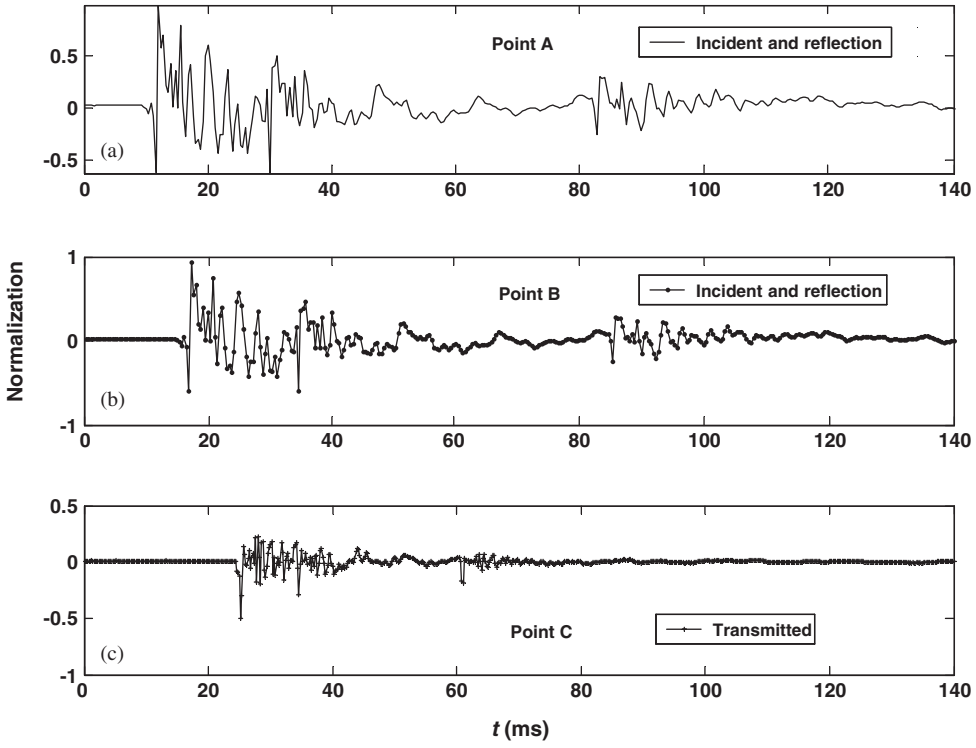

Fig. 15. Experimental results for flexural waves in a stepped beam structure.

Comparisons of the peak amplitudes shown in Fig. 15 yield

$$\gamma_{\text{Stress}} \approx 0.4, \quad \left|\frac{D}{B}\right| \approx 0.21, \quad \left|\frac{F}{B}\right| \approx 0.50. \tag{35}$$

In general, the agreement between predicted and measured results is quite good.

4. Conclusions

In this paper, a new numerical method is introduced to describe the time-domain evolution of wave packets in a stepped beam structure. The acoustical wave propagator (AWP) is derived and implemented by combining the Chebyshev polynomial expansion and fast Fourier transformation. Numerical accuracy of the AWP method is examined and compared with the exact analytical solutions. This scheme is found to be accurate and computationally effective for the prediction of the time-domain evolution of acoustical waves. In addition, the time-domain wave propagation, reflection and transmission coefficients, energy flow and transmission efficiency in one-dimensional discontinuity structures with two semi-infinite and finite structures are derived, respectively. These predicted results were compared with those obtained experimentally, and there was found to be very good agreement between the predicted and measured results.

Acknowledgements

The authors are grateful to Dr. K.S. Sum for his assistance with the experimental setup and Mrs. Lisa Cluett for her valuable discussion. The first author would like to thank the Hong Kong Polytechnic University' support from the HK Polytechnic Postdoctoral Fellowship, and the University of Western Australian for the financial support from the University Whitfeld Fellowship. Special thanks to the constructive comments from the reviewer.

Reference

[1] H. Sato, Free vibration of beams with abrupt changes of cross-section, *Journal of Sound and Vibration* 89 (1983) 59–64.
[2] J.F. Doyle, A spectrally formulated finite element for longitudinal wave propagation, *International Journal of Analytical and Experimental Modal Analysis* 3 (1998) 1–5.
[3] S. Gopalakrishnan, M.T. Martin, J.F. Doyle, A matrix methodology for Structural analysis of propagation in multiple connected Timoshenko beams, *Journal of Sound and Vibration* 158 (1992) 11–24.
[4] U. Lee, Spectral element analysis of the structures under dynamic distributed loads, in: *Proceedings of 37th AIAA/ASME/ASCE/AHS/ASC Structural Dynamics and Material Conference*, Salt Lake, Utah, USA, 1996, pp. 1605–1614.
[5] U. Lee, Equivalent continuum representation of lattice beams: spectral element approach, *Engineering Structures* 20 (1998) 587–592.
[6] U. Lee, Vibration analysis of one-dimensional structures using the spectral transfer matrix method, *Engineering Structures* 22 (2001) 681–690.
[7] C.H. Wang, L.R.F. Rose, Wave reflection and transmission in beams containing delamination and inhomogeneity, *Journal of Sound and Vibration* 264 (2003) 851–872.
[8] S.Z. Peng, J. Pan, Acoustical wave propagator for time-domain flexural waves in thin plates, *Journal of the Acoustical Society of America* 115 (2004) 467–474.
[9] S.Z. Peng, J. Pan, A study of time-domain dynamic stress concentration in a plate with a sharp change of section using acoustical wave propagator technique, *Journal of the Acoustical Society of America* 117 (2005) 492–502.
[10] S.Z. Peng, Flexural wave scattering and dynamic stress concentration in a heterogeneous plate with multiple cylindrical patches by acoustical wave propagator technique, *Journal of Sound and Vibration* 286 (2005) 743–749.
[11] S.Z. Peng, Dynamic stress concentration in a ribbed plate using acoustical wave propagator technique, *Journal of Sound and Vibration* 279 (2005) 75–88.
[12] S.Z. Peng, J. Pan, Vibration analysis of one-dimensional structures with discontinuities using the improved acoustical wave propagator technique, in: *Proceedings of ICA2004, The 18th International Congress on Acoustics,* Kyoto, Japan, 2004, pp. 2931–2934.
[13] J. Pan, J.B. Wang, Acoustical wave propagator, *Journal of the Acoustical Society of America* 108 (2000) 481–487.
[14] L. Cremer, M. Heckl, E.E. Ungar, *Structure-Borne Sound*, Springer, Berlin, 1973.
[15] K.F. Graff, *Wave Motion in Elastic Solids*, Clarendon Press, Oxford, 1975.
[16] S.Z. Peng, Acoustical Wave Propagator Technique for Structural Dynamics, PhD Thesis, 2005.
[17] B.R. Mace, Wave reflection and transmission in Beams, *Journal of Sound and Vibration* 97 (1984) 237–246.
[18] A.L. Stiehl, Power flow analysis of beam members with multiple wave types, *Finite Elements in Analysis and Design* 21 (1996) 253–264.
[19] Z.H. Wang, J.T. Xing, W.G. Price, Power flow analysis of indeterminate rod/beam systems using a substructure method, *Journal of Sound and Vibration* 249 (2002) 3–22.
[20] X. Zhao, N. Vlahopoulos, A hybrid finite element formulation for mid-frequency analysis of systems with excitation applied on short members, *Journal of Sound and Vibration* 237 (2000) 181–202.
[21] X. Zhao, N. Vlahopoulos, A basic hybrid finite element formulation for mid-frequency analysis of beams connected at an arbitrary angle, *Journal of Sound and Vibration* 269 (2004) 135–164.